

The distance to the giant elliptical galaxy M 87 and the size of its stellar subsystem *

N.A. Tikhonov¹, O.A. Galazutdinova¹, G.M. Karataeva²

¹ Special Astrophysical Observatory, Nizhnij Arkhyz, Karachai-Cherkessian Republic, Russia 369167;
ntik@sao.ru

² Astronomical Institute, St. Petersburg State University, Petrodvorets, 198504 Russia

Abstract Stellar photometry in nine fields around the giant elliptical galaxy M 87 in the Virgo cluster is obtained from archival images of the Hubble Space Telescope. The resulting Hertzsprung–Russell diagrams show populated red-giant and AGB branches. The position of the tip of the red-giant branch (the TRGB discontinuity) is found to vary with galactocentric distance. This variation can be interpreted as the effect of metal-rich red giants on the procedure of the measurement of the TRGB discontinuity or as a consequence of the existence of a weak gas-and-dust cloud around M 87 extending out to 10′ along the galactocentric radius and causing *I*-band absorption of up to 0^m.2 near the center of the galaxy. The TRGB stars located far from the M 87 center yield an average distance modulus of $(m - M) = 30.91 \pm 0.08$, which corresponds to the distance of $D = 15.4 \pm 0.6$ Mpc. It is shown that stars in the field located between M 86 and M 87 galaxies at angular separations of 37′ and 40′ are not intergalactic stars, but belong to the M 87 galaxy, i.e., that the stellar halo of this galaxy can be clearly seen at a galactocentric distance of 190 kpc. The distances are measured to four dwarf galaxies P4anon, NGC 4486A, VCCA039, and dSph-D07, whose images can be seen in the fields studied. The first three galaxies are M 87 satellites, whereas dSph-D07 is located at a greater distance and is a member of the M 86 group.

Key words: galaxies; clusters; individual; Virgo-galaxies; individual; M87

1 INTRODUCTION

As a result of the gravitational interaction between neighboring galaxies in the densely populated Virgo cluster stellar peripheries should be “stripped” from galaxies and intergalactic stars should appear (Rudick et al. 2006). Interaction processes should also alter the morphology of the stellar subsystems of galaxies, especially their extended halos. However, our analysis of galaxies in several fields of the Virgo cluster whose images were taken with the Hubble Space Telescope revealed that the stellar subsystem of each

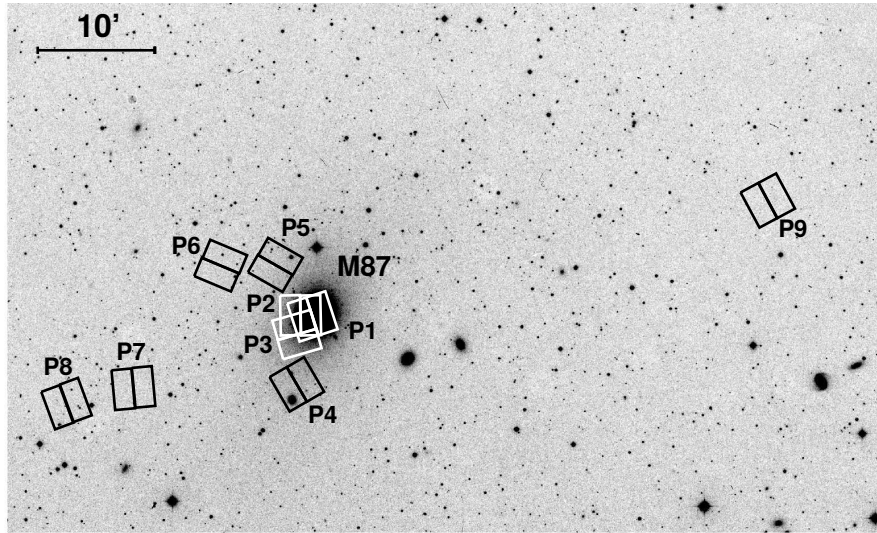


Fig. 1: Image of the part of the Virgo cluster with the M 87 galaxy in the DSS photo. The squares indicate fields P1–P9 as observed with the ACS/WFC camera of the Hubble Space Telescope. North is at the top.

the corresponding images. Finding likely intergalactic stars among numerous stars of the periphery of the galaxies, proving their intergalactic status, and determining their parameters is an extremely challenging task.

Deep Hubble Space Telescope images have been obtained for very few fields in the Virgo cluster. One of these fields, which [Williams et al. \(2007a\)](#) analyzed to search for and study intergalactic stars, is located between the two giant elliptical galaxies M 86 and M 87 at the angular separations of $37'$ and $40'$ respectively, which correspond to about 170 and 190 kpc for the adopted Virgo cluster distance of 16.5 Mpc. The location of this field was chosen based on an analysis of deep Virgo cluster images ([Mihos et al. 2005](#)) taken with the 0.6-m Schmidt telescope and reaching the 29^m arcsec $^{-2}$ B -band isophote. These and later images obtained by the same authors ([Mihos et al. 2017](#)) show that the considered field is located beyond the extended halos of the two neighboring galaxies M 86 and M 87. However, [Janowiecki et al. \(2010\)](#) analyzed the same images ([Mihos et al. 2005](#)) and found that the halo of M 87 extends out to $40'$, i.e., that the field in question should be located within the M 87 halo.

While studying the images obtained with the Hubble Space Telescope [Williams et al. \(2007a\)](#) took into account the conclusions of [Mihos et al. \(2005\)](#) and assumed that the field considered was located far enough from the giant galaxies for their contribution to the star sample to be negligible, and therefore attributed the inferred stellar parameters to intergalactic stars of the Virgo cluster.

The discovery of intergalactic stars in the Virgo cluster was reported earlier by [Caldwell \(2006\)](#), who studied two fields in the images obtained with the ACS/WFC camera of the Hubble Space Telescope. We analyzed the same observational data and concluded that intergalactic stars are totally lacking or extremely scarce ([Tikhonov 2017](#)). We therefore considered it necessary to investigate the field from [Williams et al.](#)

Tikhonov (2017) showed that the distribution of stars of neighboring galaxies has to be studied to determine whether stars in a certain field are members of a certain galaxy. The surface photometry method used in Mihos et al. (2005) to determine the structure of haloes around galaxies cannot be applied to isophotes fainter than 29–30^m and does not make it possible to determine the type of stars that form the particular halo. We therefore use the method of star counts and complement the study of the field of Williams et al. (2007a), which denote here as P9, by investigating eight more fields around the M 87 galaxy that are resolvable into stars (Fig. 1) in order to study the variation of the parameters of stars with galactocentric distance. The results obtained led us to a conclusion about the nature of stars in field P9, which we report in this paper.

According to the NASA Extragalactic Database¹ (NED), the elliptical galaxy M 86 is fainter than M 87 and has a smaller-sized stellar subsystem. However, field P9 (Fig. 1) is located along the major axis of M 86, where the size of its stellar halo is the greatest. Therefore stars in the considered field can be both intergalactic objects or belong to the periphery of the M 86 and M 87 galaxies. The ratio number of stars belonging to different galaxies in this field can be measured by performing stellar photometry of this field and the neighboring galaxies.

The principle indicator of the membership of a star in the considered field in a particular galaxy is the equal distance to both the galaxy and to the stars of the considered field (provided that the stars are not broadly distributed along the line of sight). The TRGB (Tip of Red Giants Branch) method Lee et al. (1993), which allows the distance to a group of red giants to be determined sufficiently accurately and reliably is probably the only method for determining the distance in the considered case.

2 CHOICE OF FIELDS AND STELLAR PHOTOMETRY

To study the space structure of stellar subsystems in the M 86 and M 87 galaxies of the Virgo cluster and determine accurate distances and study intergalactic stars, we used archival images taken by the Hubble Space Telescope (HST) within the following applications: ID 10131, 10543, 12532, 12989, and 13731. The main criterion for the choice was that the *F814W* (*I*)-band ACS/WFC exposure should be 2000 seconds or longer. We did not require the availability of images of the same field taken with another filter, although we consider such images to be useful. We found deep images of a total of nine fields, which we hereafter refer to as P1–P9, located at different distances from M 87. We also found four fields for M 86, however, photometry showed that this galaxy is 2.0–2.5 Mpc farther way than stars of field P9, and we therefore do not consider it in this study. We show the location of fields P1–P9 with respect to the M 87 galaxy in the DSS (Digital Sky Survey) image in Fig. 1, and HST archival images in Fig. 2.

We should point out the heterogeneity of the data used. For fields P1, P5, and P9 we have deep *F814W* (*I*) and *F606W* (*V*)-band images, and this is optimal for distance measurement. Less deep *F814W* (*I*) and *F475W* (*B*)-band images are available for the other fields (see Table 1, which summarizes the data about image exposures and filters). The distances determined using the TRGB method rely on red giants, which are near the photometric limit in the images taken with the blue filter *F475W* (*B*), but are quite conspicuous in the images taken with the *F814W* (*I*) filter. Combined photometry of *F814W*- and

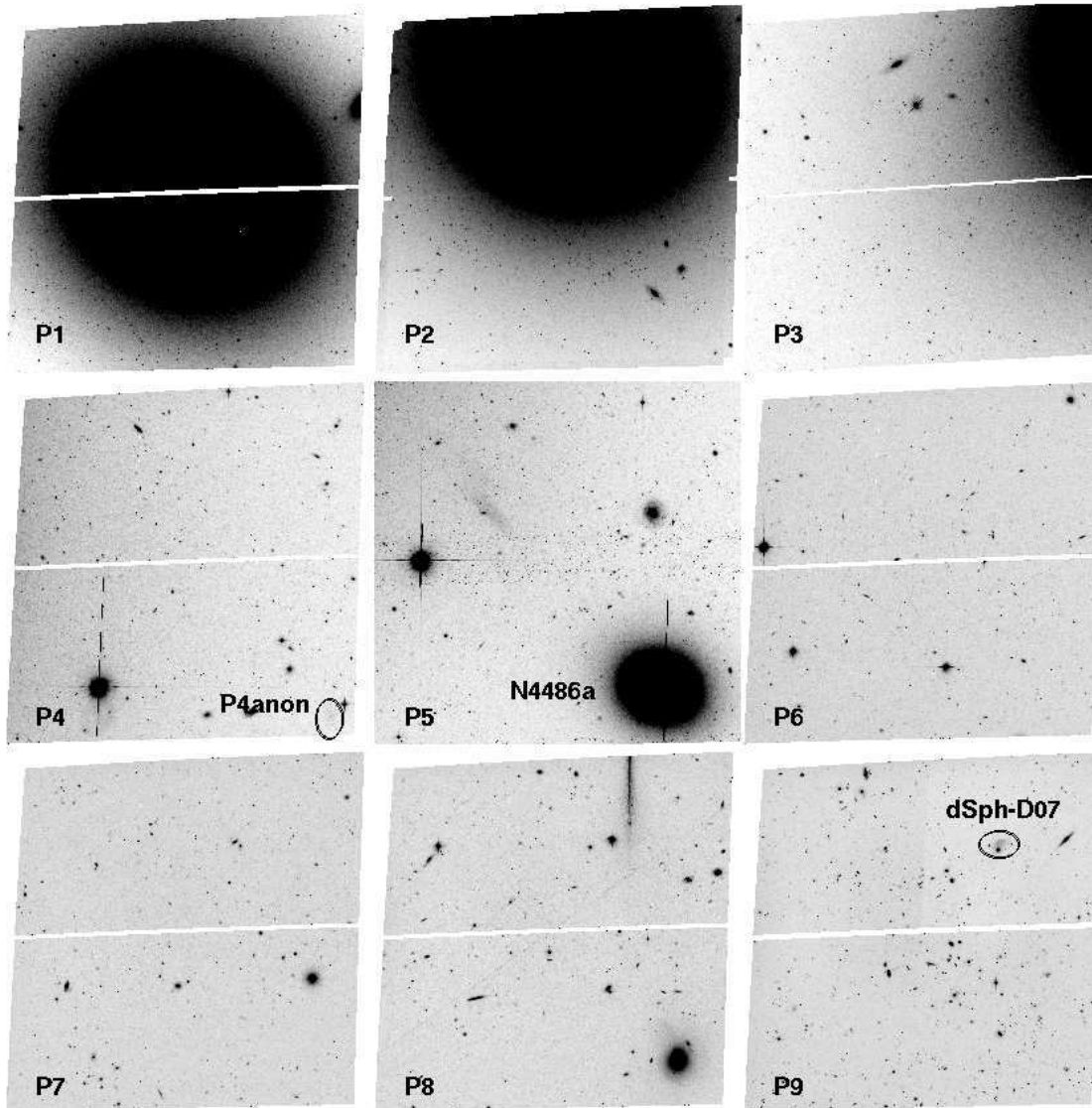


Fig. 2: Fields P1–P9 on Hubble Space Telescope images. The ellipses in fields P4 and P9 indicate dwarf galaxies. All images have the size of $3'5 \times 3'5$.

Table 1: Exposures of P1—P9 field images (in seconds)

Filter	P1	P2	P3	P4	P5	P6	P7	P8	P9
<i>F814W</i> (<i>I</i>)	73800	4270	2589	2282	12860	2282	2282	2282	26880
<i>F606W</i> (<i>V</i>)	24500	–	–	–	12050	–	–	–	63440
<i>F475W</i> (<i>B</i>)	–	–	2729	2351	–	2351	2351	2351	–

F475W-band images, as it is done in DOLPHOT package [Dolphin \(2016\)](#), sets the common photometric limit based on the less deep *F475W*-band image. DAOPHOT II ([Stetson 1987, 1994](#)) package of MIDAS provides sufficient amount of stellar photometry in the deepest *F814W*-band filter, allowing the TRGB discontinuity to be determined from deeper images, although the lack of star color information somewhat

Table 2: Aperture sizes used for DAOPHOT II photometry of ACS/WFC HST images

Aperture	A1	A2	A3	A4	A5	A6	A7	A8	A9	AA	AB	AC	IS	OS
Radius, pixels	1.5	1.7	2.0	2.4	2.9	3.5	4.2	5.0	5.8	7.9	8.5	10.0	12	20

We performed stellar photometry in a standard way using DAOPHOT II software, as described in our earlier paper [Tikhonov et al. \(2009\)](#). For aperture photometry we used smaller than recommended standard aperture sizes (Table 2) to ensure more crowded arrangement and more precise description of the photometric profile at the centers of the stars.

We selected the results of our stellar photometry by parameters “ $CHI < 1.5$ and “ $|SHARP| < 0.3$, which determine the shape of the photometric profile of each measured star ([Stetson 1987](#)), making it possible to eliminate from photometric tables all diffuse objects—star clusters, distant or compact galaxies—because profiles of these objects differ from those of isolated stars selected as standards.

We used DOLPHOT 2.0 package² in accordance with the recommendations given in the manual. The procedure of photometry consisted of preliminary masking of “bad” pixels, cosmic-ray hit removal, and subsequent PSF photometry of extracted stars in two filters. Selection of stars from the resulting preliminary list by image-profile parameters “ CHI ” and “ $|SHARP|$ ” was performed in the same way as in DAOPHOT II. To perform photometry of stars in the central region of the M 87 galaxy (field P1), we aligned and averaged more than 200 images. However, despite very long exposure, the photometric limit of the images in the central part of this field is much shallower because of the strong crowding of stars and the brightness of the galaxy.

The use of the sole filter ($F814W$) for determining the TRGB discontinuity and computing the distance to a galaxy has its certain unique features. Given that it is impossible to obtain a Hertzsprung–Russell diagram (the CM diagram) to identify red giants by color, the resulting luminosity function refers to all field objects. If the field contains many metal-poor red giants then the TRGB jump is always quite conspicuous even in the case where an image taken in one filter is used. However, if the star sample consists of a mix of metal-rich and metal-poor stars, which is the case in elliptical galaxies, the TRGB discontinuity shows up only as the variation of the gradient of the luminosity function. In many cases such a variation of the gradient is more conspicuous if logarithmic scale is used for the number of stars.

We used the following equations to transform instrumental magnitudes into the Kron–Cousins V - and I -band magnitudes in DAOPHOT II:

$$(V - I) = 1.3213(v - i) + 1.133, \quad (1)$$

$$I = i + 0.0592(V - I) + 25.972, \quad (2)$$

where $(v - i)$ and i are the instrumental magnitudes and $(V - I)$ and I are the magnitudes in the corresponding passbands of the Kron–Cousins system. We derived the above equations based on photometry of the same stars carried out with different telescopes and detectors: 6-m telescope of the Special Astrophysical Observatory of the Russian Academy of Sciences, 1-m Zeiss-1000 telescope, and the Hubble

Table 3: Accuracy of $F814W$ -band stellar photometry in fields P1–P9 around M 87

m^*	P1	P2	P3	P4	P5	P6	P7	P8	P9
25	0.02	0.05	0.03	0.02	0.04	0.03	0.03	0.05	0.02
26	0.04	0.08	0.05	0.04	0.07	0.06	0.05	0.07	0.02
27	0.12	0.15	0.10	0.13	0.14	0.14	0.12	0.14	0.03
28	0.30	0.35	0.25	0.32	0.30	0.32	0.28	0.33	0.07

* m — apparent magnitude in the $F814W$ filter

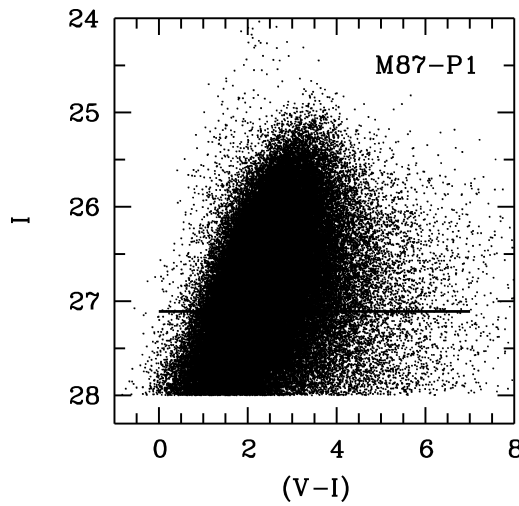


Fig. 3: Color-magnitude diagram for the central field (P1) of the M 87 galaxy. The horizontal line indicates the upper boundary of the red-giant branch—the TRGB discontinuity. The domain of very bright AGB stars is located above the TRGB discontinuity.

Space Telescope with WFPC2 camera (Tikhonov and Galazutdinova 2009). The transformation equations are accurate to within 0^m02 and 0^m03 for I -band magnitude and $(V - I)$ color index, respectively.

The second equation shows a weak dependence of the resulting I -band magnitude on $(V - I)$ color index. Hence the use of the average color index $(V - I) = 1.6$, which is close to real colors of red giants in elliptical galaxies, should result in extra error of only 0^m01 for stars that are 0^m2 bluer or redder. It is clear that such transformation cannot be used for simultaneous reduction of instrumental magnitudes to I -band magnitudes for blue and red stars, however, no blue stars are present in the fields where photometry was performed.

Photometry in fields P2–P9 was performed with DAOPHOT II, and photometry in fields P1, and P4–P9 was additionally performed using DOLPHOT package. The accuracy of stellar photometry performed in the $F814W$ filter is given in Table 3.

We determined Galactic foreground extinction towards fields P1–P9 in accordance with Schlafly and Finkbeiner (2011). Extinction is small towards all fields and varies from $A_I = 0^m040$ for field P8 to

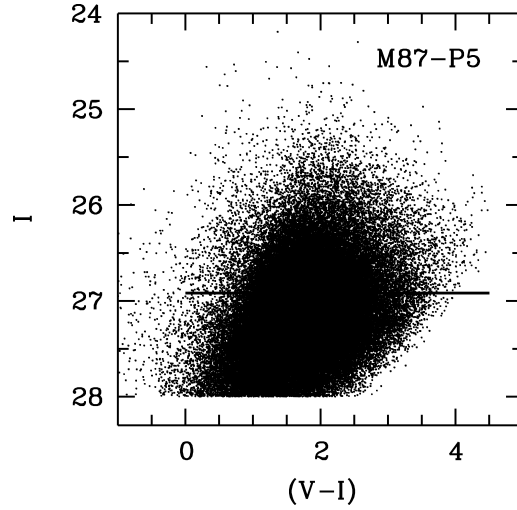


Fig. 4: Color-magnitude diagram for stars in field P5. The horizontal line indicates the location of the TRGB discontinuity. Very bright AGB stars are practically absent, but there are quite a few intermediately bright AGB stars.

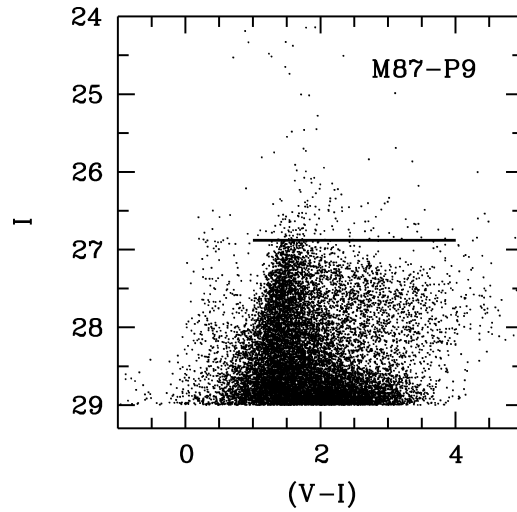


Fig. 5: Color-magnitude diagram for stars in field P9. Almost vertical branch of metal-poor red giants can be seen at $(V - I) = 1^m5$. The horizontal line indicates the TRGB discontinuity on this branch. Metal-rich red giants are located in the domain with magnitudes from $I = 27^m2$ to $I = 28^m5$ and color indices $(V - I)$ from 2^m0 to 4^m5 . A small number of low-luminosity AGB stars are located above the TRGB discontinuity.

3 STELLAR SUBSYSTEMS M87

Figures 3, 4, and 5 show the color-magnitude diagrams of fields P1, P5, and P9. The diagram for field P1 (Fig. 3) contains many very bright AGB stars located above the TRGB discontinuity, which for this field is equal to $I = 27.10$. Given that such a diagram is typical for any bright elliptical galaxy it is absolutely unclear how Bird et al. (2010), based on their photometry of the same images, left only red giants on their color-magnitude diagram removing all brighter AGB stars. Besides AGB stars, the color-magnitude diagram in Fig. 3 contains many metal-rich red giants whose color indices extend to $(V - I) = 6^m0$. The color-magnitude diagram of field P5, which is farther away from the center of the galaxy than field P1,

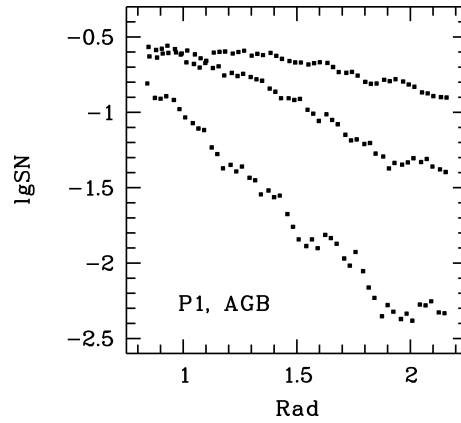


Fig. 6: Distribution of the number density of AGB stars of different luminosity along the galactocentric radius in the central field P1. The higher the luminosity of stars, the higher is the gradient of the density decrease. Then horizontal axis gives the angular distance from the center of M 87 in arcmin.

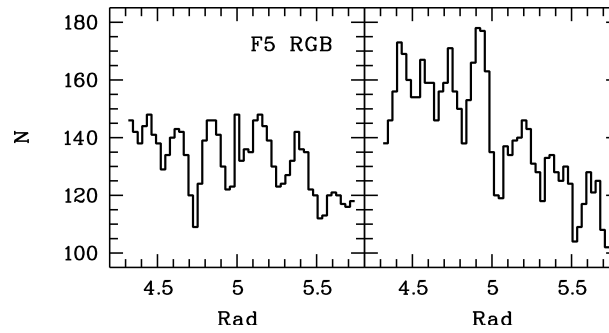


Fig. 7: Distribution of the number density of red giants of different metallicities along galactocentric radius in field P5. Metal-poor red giants show lower radial density decline gradient than higher-metallicity giants, and this results in the variation of morphology of the star sample along galactocentric radius. The horizontal axis gives the distance from the center of M 87 in arcmin.

photometrically deepest among the fields considered. Its color-magnitude diagram features the branch of metal-poor red giants and also a small domain of metal-richer red giants. There are very few AGB stars in this field. The weak branch of blue objects at $(V - I) = 0^m.4$ is made up of foreground objects and is not associated with M 87. Stars in field P9 have the most accurate photometry and hence yield the most precise measurement of the position of the TRGB discontinuity and the distance to M 87.

Figure 6, which shows the variation of the number density of AGB stars of different luminosity along the galactocentric radius in field P1. It is evident from the figure that the higher the luminosity of stars the steeper is the gradient of the decrease of the number density. The behavior stars in accordance with the diagram in Fig. 6 means that no very bright AGB stars can be seen relatively close to the center of M 87. At large galactocentric distances even intermediately-bright AGB stars become scarce and the color-magnitude diagrams in Figs. 3, 4, 5 fully corroborate this fact.

Figure 7 shows the diagram of the variation of the number density of metal-poor and metal-rich red giants along galactocentric radius. As is evident from the figure, metal-poor giants show a less steep distribution along galactocentric radius. This dependence results in the variation of the proportion of metal-poor and

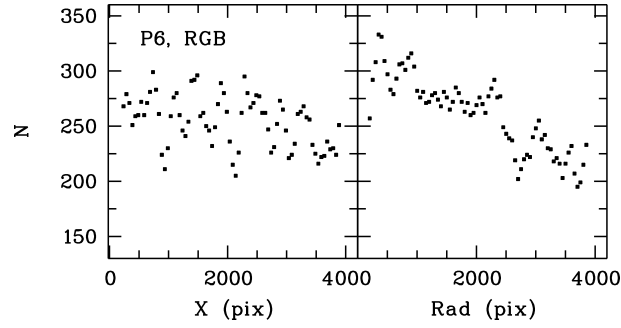


Fig. 8: Distribution of the number density of red giants in field P6 perpendicularly to the radial direction of M 87 and along this direction. The small gradient of the distribution in panel (a) can be explained by the not very accurate positioning of field P6 along the radial direction.

change of behavior with stellar metallicity. This means that the space distribution laws for intermediate-metallicity stars should be intermediate between those of metal-poor and metal-rich stars.

The differences between the gradients of the decline of the number density of stars of different types result in the variation of color index along the radius. [Montes et al. \(2014\)](#) used such photometric variations to compute the metallicity and age of stars along galactocentric radius. This method allows us to trace the color variations in the central region of M 87, but it remains “blind” for interpreting the population type in this region because instruments detect only the sum of the intensities of stars of all types in the region considered without making it possible to separate, e.g., the contributions of high- and low-luminosity AGB stars because they have almost identical color indices.

The M 87 membership of stars in fields P1–P5 is beyond question given the presence of the galaxy in the images, but M 87 cannot be seen in fields P6–P9. Can stars in these fields belong to other galaxies? Partially can, because, e.g., in fields P7 and P9 there are two dwarf galaxies with our distance estimates. However, the bulk of the stars in fields P6–P9 belong to M 87. We constructed the distribution of the number density of red giants toward the direction perpendicular to the radius of M 87, and the corresponding distribution along the radius for field P6 and for the outermost field P9 (Figs. 8 and 9). The increase of the number of stars toward M 87 and the uniform distribution of these stars in the perpendicular direction are immediately apparent. These diagrams combined with the fact that the distances to different fields around M 87 are the same, as we will show below, prove conclusively the membership of AGB stars and red giants in these fields in extended stellar subsystems M 87. Projections of dwarf galaxies introduce minor distortions into this global structure, but this does not alter the general conclusion that the stellar periphery in M 87 extends out to a radius of $40'$ and appears to extend even farther judging by the number of stars in the outermost field.

Massive galaxies are known to have extended stellar halos ([Tikhonov et al. 2005](#); [Rudick et al. 2010](#); [Rejkuba et al. 2014](#); [Ibata et al. 2014](#)), which are observed around the galaxies either using the methods of surface photometry or by measuring the number density of stars, provided that the galaxy can be resolved into stars. Measurements of some giant galaxies revealed that they possess extensive stellar halos. [Rejkuba et al. \(2014\)](#) traced the extent of the stellar periphery out to 140 kpc in the NGC 5128 galaxy in Centaurus cluster, which is less luminous than the galaxies M 86 and M 87 in Virgo cluster. [Mihos et al. \(2013\)](#) per-

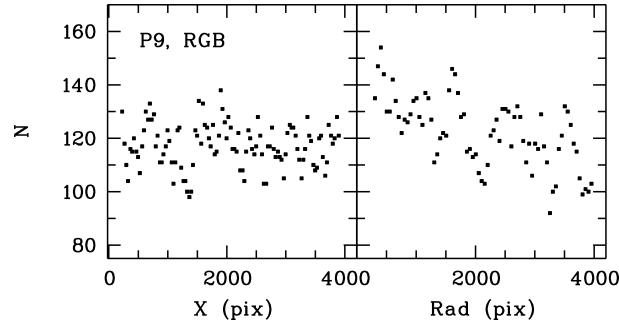


Fig. 9: Same as in Fig. 8, but for field P9. The observed uniform distribution of the number of stars in the direction perpendicular to the radius of M 87 (the X-axis) and the increase of the number of stars along this direction indicate that stars in field P9 belong to the periphery of the M 87 galaxy.

distance of 100 kpc. [Kormendy et al. \(2009\)](#) estimated the size of the stellar periphery of M 87 and found its stellar component to extend out to 200 kpc. [Oldham and Auger \(2016\)](#) used the results of [Kormendy et al. \(2009\)](#) in their proposed model of the structure of M 87 and estimated the size of its stellar component to be 1 Mpc. Naturally, no real measurements can confirm or disprove this estimate because the presence of bright neighboring galaxies makes it impossible to measure the extremely faint halo at such a galactocentric distance even if it is actually present there.

Note that the surface brightness method can be used in clusters of galaxies only down to a certain isophote. Because of the high concentration of galaxies, effects arising when different galaxies located far apart are projected onto the same field, and possible glow of intergalactic objects: stars ([Ferguson et al. 1998](#); [Durrell et al. 2002](#); [Williams et al. 2007a](#)), planetary nebulas ([Arnaboldi et al. 2002](#); [Mihos et al. 2009](#); [Longobardi et al. 2015](#)), and globular clusters ([Williams et al. 2007b](#); [Ko et al. 2017](#)), moving to very deep brightness levels would result in the isophotes of all objects merging into a single large cloud. In this case it will be impossible to determine the boundaries of faint isophotes of individual objects. The method of star counts for measuring the sizes of galaxy halos is barely affected by background and foreground objects, but it requires deep images, which cannot always be acquired.

4 MEASUREMENT OF DISTANCE

The distances to the M 86 and M 87 galaxies have been measured repeatedly using different methods. The NED database contains more than one hundred distance estimates. The mean and median distance estimates are equal to 16.08 and 16.80 Mpc, respectively, for M 86 and 16.56 and 16.40 Mpc, respectively, for M 87 (NED). Some methods, e.g., the one based on planetary nebulas, yield smaller-than-average estimates (14.6 Mpc for M 87), and the method based on the brightness of novae yields greater-than-average estimates (18.8 Mpc for M 87). This appears to be due to the calibration of the respective zero points and the extensive program aimed at the study of novae in M 87 ([Shara et al. 2016, 2017](#)) will change the situation.

The NED database contains the results of measurements made using all methods with different accuracy, and therefore to determine the true distances we should rely on the TRGB method, which is currently considered to be the most precise among the methods applied for elliptical galaxies. This method yielded the following distance estimates for M 87: 15.1 Mpc ([Lee and Jang 2016](#)), 15.2 Mpc ([Ferrarese et al.](#)

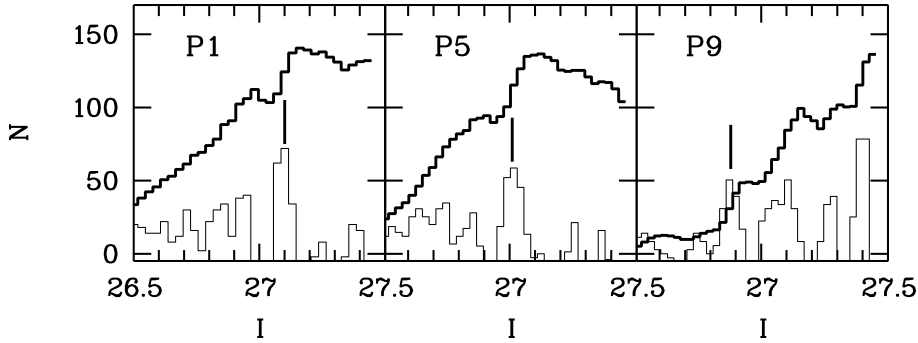


Fig. 10: Luminosity functions of stars near the boundary of the red-giant branch for fields P1, P5, and P9. Because of the presence of stars of different metallicities in the sample the TRGB discontinuity is observed on the luminosity function shows up as the variation of the gradient. The thin line shows the Sobel function, which indicates maximum gradients of the luminosity function. The vertical bars indicate the positions of TRGB discontinuities, which for the given sample correspond to the boundary of red giants.

reject the evident outlier—19.4 Mpc—then the average distance estimate becomes 15.75 Mpc. Note that the TRGB method-based distance measurements in the above papers in each case relied on the data for a single field. Such measurements are quite sufficient for most of the galaxies, but, as our measurement showed, for M 87 several fields located at different galactocentric distances have to be used.

No TRGB-based distance measurements for M 86 are available in NED, but our earlier estimates (Tikhonov 2017) as well as new distance estimates based on four fields indicate that M 86 is located about 2 Mpc farther than M 87. If field P9 located between M 86 and M 87 contains stars of both galaxies then we have to observe two separate TRGB discontinuities on the luminosity function of red giants.

The color-magnitude diagrams of M 87 fields (Figs. 3, 4, 5) contain red giants, which at galactocentric separations smaller than $10'$ are masked by brighter AGB stars. The presence of red giants makes it possible to use the TRGB method in accordance with Lee et al. (1993) for distance measurement. To determine the position of the upper tip of the red giant branch we applied the Sobel filter (Madore and Freedman 1995) to the luminosity function of red giants and AGB stars. The maxima of the Sobel filter indicate the locations of abrupt change of the luminosity function gradient, which is observed when passing from AGB stars to the beginning of the red-giant branch. The TRGB discontinuity is hardly visible in the case of giant elliptical galaxies because the sample studied includes stars of different metallicity. In this case, the variation of gradient of the luminosity function is observed instead of the TRGB discontinuity. The position of the TRGB discontinuity in the I -band filter depends slightly on the metallicity of red giants, and therefore it is necessary to know the metallicity of these stars. In the method of Lee et al. (1993) metallicity is measured via two quantities: $(V - I)_{\text{TRGB}}$, the color index of the tip of the red giant branch, and $(V - I)_{-3.5}$, the color index of the red-giant branch at the $M_I = -3.5$ level. Once the location of the TRGB discontinuity on the luminosity function and the color indices of the red-giant branch on the color-magnitude diagram are determined, the distance to the galaxy studied can be computed as described in Lee et al. (1993).

Figure 10 presents the luminosity functions for stars in fields P1, P5, and P9. Despite long exposures in field P1 the TRGB discontinuity can be seen only on the luminosity function of stars located farther

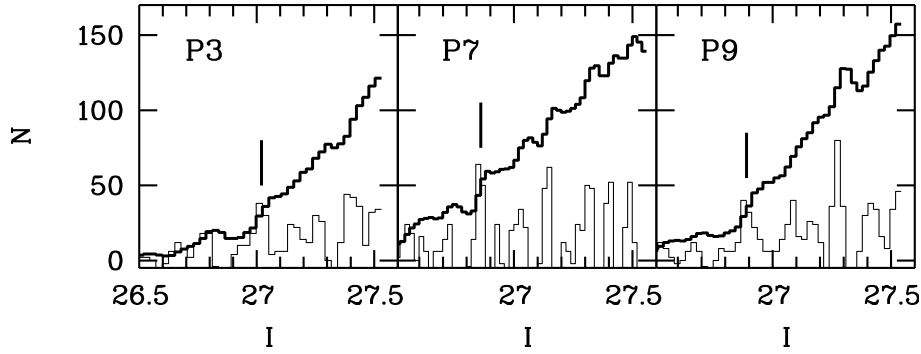


Fig. 11: Luminosity functions for fields P3, P7, and P9. Unlike Fig. 10, where the sample of stars was subjected to $(V - I)$ color cut, the luminosity functions presented here are based on photometry in the sole I -band filter. A comparison of the diagram for field P9 with the corresponding diagram in Fig. 10 shows their similarity, i.e., confirms the possibility of measuring the TRGB discontinuity based on stellar photometry in the sole I -band filter .

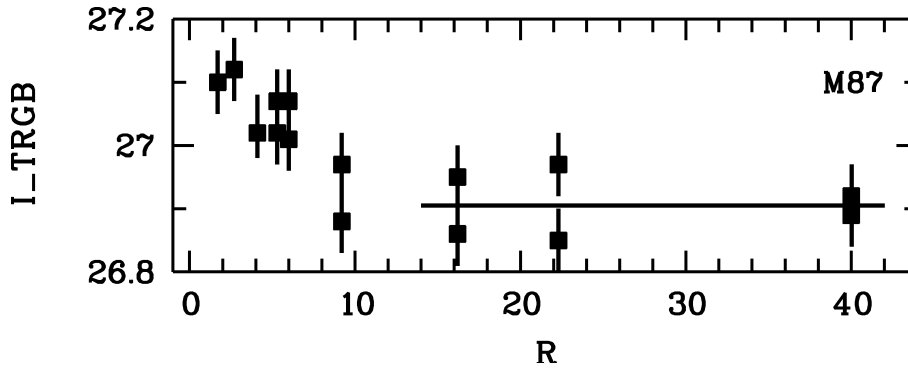


Fig. 12: Variation of the position of the TRGB discontinuity on the stellar luminosity function with the distance of the considered field from the center of the galaxy. We appear to see the effect of metal-rich red giants whose number decreases with the distance from the center of the galaxy. No systematic variation of the TRGB discontinuity occurs beyond the $10'$ radius and therefore the results for fields P7–P9 yield the real distance estimate to M87.

stars that red giants are lost amongst brighter and more numerous AGB stars. The change of the gradient of the luminosity function for stars of this field (the TRGB discontinuity) is observed at $I = 27.10$. The luminosity function for stars of field P5, located farther away from the center of the galaxy, changes its gradient at $I=27.01$, which is the TRGB discontinuity. For an even more distant field P9, a change in the gradient of the luminosity function can be seen at $I = 26.89$.

Figure 15 shows the luminosity functions for fields P3, P7, and P9. The luminosity function for field P9 is based on the results of single-band (I) stellar photometry. A comparison with Fig. 10, where a similar luminosity function is based on photometry on two filters and selection of red giants based on the color-magnitude diagram, shows no difference in the resulting measured TRGB discontinuity. Hence images taken with the sole I -band filter are quite sufficient for determining the TRGB discontinuity, provided,

We present the results of all measurements in Table 4 and in Fig. 12. Paired TRGB discontinuity values for each radius are due to the use of two software packages—DAOPHOT and DOLPHOT—for performing photometry in each field. The variation of the TRGB discontinuity from $I = 27.1$ to 26.9 with the distance from the center of the galaxy is immediately apparent in Fig. 12. At radii greater than $10'$ the TRGB discontinuity value remains unchanged within the measurement errors. We discuss the possible causes of such variation in section 6. But in any case the most reliable distance estimates can be obtained from the results of photometry in fields P7–P9.

We used the results of photometry in these fields to find the mean distance modulus of M 87 based on six measurements in three fields and corrected for Galactic foreground extinction ($m - M$) = 30.91 ± 0.08 , which corresponds to the distance of $D = 15.39 \pm 0.57$ Mpc. Such a distance estimate puts the M 87 galaxy to the nearest boundary of the cluster rather than into its center, if only the cluster itself is not closer to us than Fouqué et al. (2001) believed.

5 DISTANCES TO DWARF GALAXIES

Very faint galaxies projected onto M 87 and resolvable into stars can be seen in the images of fields P4 and P9 (Fig. 2). When we determine the distance to such a galaxy, the sample includes stars of two galaxies: the dwarf studied and the huge M 87 background system onto which the dwarf is projected. To increase the fraction of stars of the dwarf galaxy compared to that of stars of the background M 87 galaxy, we decreased the area of the sample for it to fit within the boundaries of the dwarf galaxy. Furthermore, when determining the TRGB discontinuity we compared the luminosity function of stars of the dwarf galaxy to that of the stars of the background area located near M 87 and containing only its stars. The most challenging case is that of the anonymous dwarf galaxy in field P4—P4 (anonymous) hereafter referred to as P4anon because of its small size and small number of stars. The sample of stars of this galaxy contains 202 objects, whereas the nearby background area contains 132 stars. Fig. 13 shows the color-magnitude diagrams for these areas. Despite the small number of stars, the TRGB discontinuity of this galaxy can be determined quite reliably and its value differs from the TRGB discontinuity of background stars, which can be determined using a larger area rather than the small sample shown in Fig. 1. The dwarf galaxy in field P9 contains only 40 stars, but the nearby comparison area contains only four stars (Fig. 14), and therefore the TRGB discontinuity is quite conspicuous and measuring the distance to this galaxy poses no problem.

The galaxies NGC 4486a (field P5) and VCCA 39 (field P7) have much greater sizes than the dwarfs in fields P4 and P9, but their central regions cannot be resolved into stars because of high star density and high brightness. We plotted the star number density distributions along the radius for these galaxies and determined the radius R_{gal} at which the density of galaxy stars becomes greater than the density of the background, which consists of M 87 stars. After determining the R_{gal} radius we selected stars for computing the luminosity function inside the ring of radius $R < R_{\text{gal}}$ and did not use the central regions. Fig. 15 shows the resulting luminosity functions for three galaxies whose distances have not been determined earlier via the TRGB method. Table 4 lists the TRGB discontinuities (I_{TRGB}) for the galaxies P4anon, NGC 4486a, and VCCA 39. The measured distances to these galaxies are equal to 15.6, 15.6, and 16.1 Mpc, respectively.

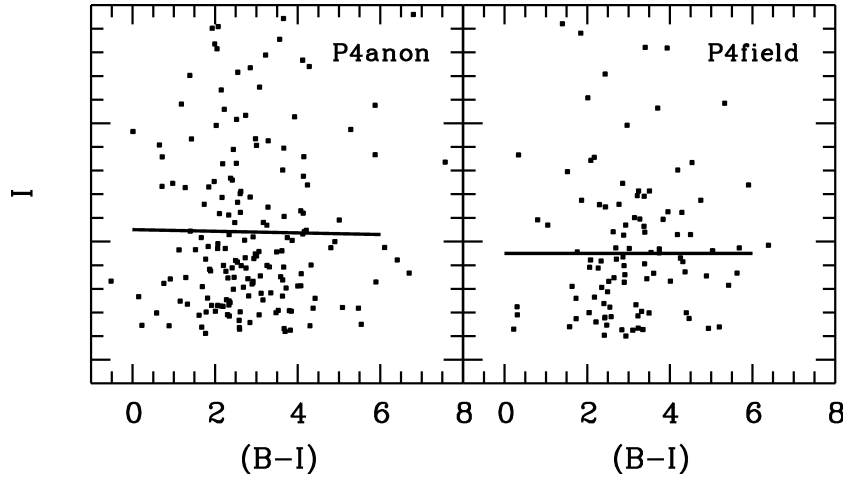


Fig. 13: Color-magnitude diagrams of the dwarf galaxy P4anon and the nearby background area. The samples of the dwarf-galaxy and background-area stars consist of 202 and 132 objects, respectively, i.e., red giants of the dwarf galaxy make up one third of the samples. The position of the TRGB discontinuity on the luminosity function of the P4anon galaxy indicates (Fig. 15) that it is located in front of the giant galaxy M 87 and is its satellite.

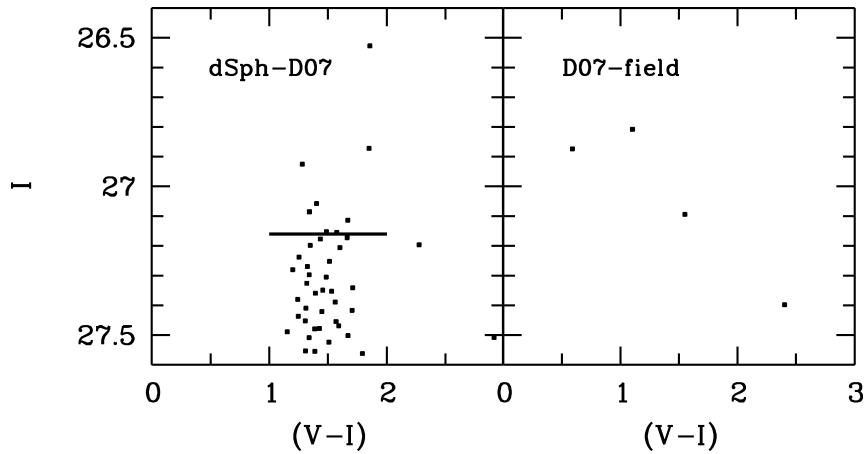


Fig. 14: Color-magnitude diagrams of the dwarf galaxy P9(dSph-D07) and the nearby background area. The samples of the dwarf-galaxy and background-area stars consist of 40 and four objects, respectively. The value of the TRGB discontinuity at $I = 27.16$ indicates that this galaxy is 2 Mpc farther from us than M 87.

the TRGB discontinuity and that of the equations used to transform this position into linear distance units. The accuracy of transformation equations (Lee et al. 1993) and that of the determination of the TRGB discontinuity are equal to $I = 0^m10$ and of about 0^m03 , respectively. The transformation equations from instrumental magnitudes to the Cousins system are accurate to 0^m02 and the accuracy of the computation of the PSF profiles of stars is about the same. The combined contribution of all measurement errors is 0^m16 , which is equivalent to the 1.3 Mpc accuracy of the distance estimates for each galaxy.

The distances to P4anon, NGC 4486a, and VCCA 39 differ little from the distance to M 87, i.e., they are satellites of the giant M 87 galaxy. The fourth dwarf galaxy that located in field P9 (dSph-D07)

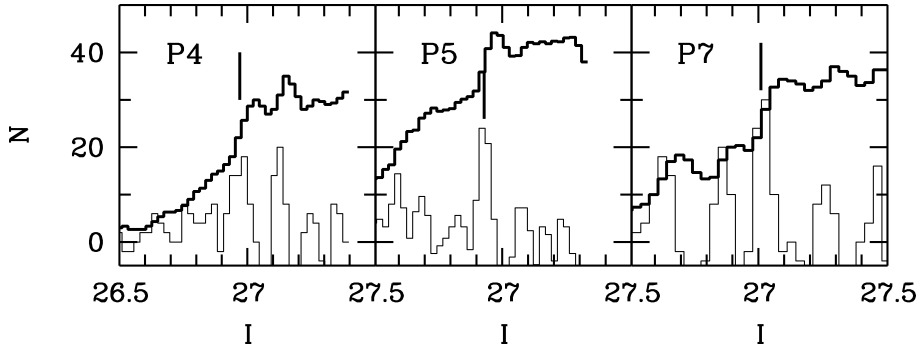


Fig. 15: Luminosity functions of the dwarf galaxies P4anon, NGC 4486A, and VCCA039. Designations are similar to those used in Figs. 10 and 11. The values of the TRGB discontinuities differ only slightly from that of M 87, i.e., these galaxies are located at the same distance as M 87 and are its satellites.

Table 4: TRGB discontinuity values in fields P1–P9 around M 87 and in dwarf galaxies

Object	P1	P2	P3	P4	P5	P6	P7	P8	P9
M 87 (DAO)*	–	27.12	27.03	27.07	27.01	26.88	26.99	26.85	26.89
M 87 (DOL)*	27.10	–	–	27.02	27.05	26.97	26.86	26.95	26.92
P4anon	–	–	–	26.97	–	–	–	–	–
NGC 4486a	–	–	–	–	26.93	–	–	–	–
VCCA 039	–	–	–	–	–	–	27.01	–	–
dSph-D07	–	–	–	–	–	–	–	–	27.16

* based on the results of DAOPHOT (DAO) and DOLPHOT (DOL) photometry

2007a), $D = 17.6 \pm 1.4$ Mpc (Durrell et al. 2007), $D = 18.3 \pm 1.4$ Mpc (Jang and Lee 2014). Our distance measurement yielded $D = 17.1 \pm 1.5$ Mpc with the red-giant metallicity of $[Fe/H] = -1.8$, which agrees with earlier measurements within the errors. This dwarf spheroidal galaxy is almost 2 Mpc farther than M 87 and belongs to the group of the more distant galaxy M 86 with $D = 18.5 \pm 0.5$ Mpc (Tikhonov 2017).

6 RESULTS AND DISCUSSION

Our aim was to investigate the parameters of stars in the area between the M 86 and M 87 galaxies and make conclusions about their origin. We concluded that the study has to be extended to investigate the structure of the M 87 subsystem and determine the space position of this galaxy in Virgo cluster.

While addressing these tasks we demonstrated the efficiency of the star count method. This is practically the only method that allows studying the morphology and stellar composition of the faint and extended periphery of a galaxy. We used the technique of star counts for several fields located at different distances from the center of M 87 to demonstrate the variation of the number density of AGB stars and red giants of various luminosities and metallicities along the galactic radius (Figs. 6 and 7). We established that the most luminous AGB stars show the largest gradient of density decrease, and that gradient decreases ‘when passing to less luminous stars. A dependence was found between the metallicity of red giants and the gradient of the variation of the star number density along the galactic radius. The results obtained explain

(P9 according to our numeration) predominantly belong to the periphery of the M 87 galaxy. So, there are no grounds to consider them to be likely intergalactic stars, and even if they are part of the sample, they still do not affect its parameters because of their small number. The fact that stars of M 87 are found at a distance of 190 kpc from its center indicates that the size of the stellar halo is not smaller than this value. It is evident from the images obtained by Mihos et al. (2005, 2017) that the halo of M 87 has a shape of a regular ellipse, and therefore the detection of halo stars at a single location in this ellipse determines the size of the entire halo up to this radius. In the diagram in Fig. 5 many stars that belong to the outermost field of M 87 can be seen. Given the smooth decrease of the stellar number density, we can conclude that the halo extends beyond this field located at a distance of 190 kpc from the center of the galaxy. Hence the size of the halo is greater than 190 kpc.

The conclusions reached in this paper and the results of our earlier studies (Tikhonov 2017) show that stars in all the Virgo cluster fields that we studied belong to the peripheries of neighboring galaxies and are not intergalactic stars as a number of studies have suggested (Caldwell 2006; Williams et al. 2007a). Apparently, the process of stripping of galaxies (Rudick et al. 2006) is not an efficient mechanism for generating intergalactic stars in clusters.

Determining the distance to the M 87 galaxy via the TRGB method revealed the variation of the TRGB discontinuity with increasing distance from the center of the galaxy (Fig. 12). This effect can be explained by the variation of the morphological composition of the star sample: fields closer to the center of the galaxy contain red giants with higher metallicity, and this is what causes the systematic shift of the TRGB discontinuity as observed in the diagram in Fig. 12.

There is another possibility, less likely cause of the observed dependence in Fig. 12. During its entire lifetime, the giant M 87 galaxy has cannibalized quite a few dwarf galaxies. Dust of these galaxies may have formed a weak halo around M 87 causing light absorption and shifting the TRGB discontinuity. This would result in fictitious increase of the distance as we go to samples located closer to the center of the galaxy. This effect can probably also explain the systematically greater distance to M 87 determined using the method based on nova stars, which explode more often in central regions of the galaxy. Extensive studies of novae in M 87 (Shara et al. 2016, 2017) will possibly resolve the problem of measuring the distance via this method. We believe that the most accurate M 87 estimates are those provided by measurements performed via the TRGB method applied to fields P7–P9 at the periphery of the galaxy.

Our distance estimate to M 87 puts this galaxy to the forefront of the cluster if only the entire cluster is not located closer than Fouqué et al. (2001) believed. The asymmetric position of M 87 in the cluster is not unexpected. For example, all measurements based on planetary nebulas yielded small distances to M 87 (NED). Recent measurements of this type include: $D = 14.1$ Mpc (Longobardi et al. 2013), $D = 14.5$ Mpc (Longobardi et al. 2015).

Three dwarf galaxies located near M 87 that happen to be in the fields studied yield approximately the same distances as M 87, thereby indirectly corroborating the correctness of our distance measurements to M 87.

M 87 does not need to be at the center of the cluster. It is by no means the brightest galaxy in

It has been repeatedly shown that Virgo cluster is a loose assembly of individual groups of galaxies (Neilsen and Tsvetanov 2000; Fouqué et al. 2001; Solanes et al. 2002; Mei et al. 2007), which near future may form a regular cluster of galaxies.

The question about the location of individual groups of galaxies inside Virgo cluster remains open because of the lack of accurate distance measurements of other massive cluster galaxies besides M 87. Numerous but not accurate measurements made using the Tully–Fisher (TF) or surface brightness fluctuations (SBF) methods cannot replace few but accurate measurements made using the TRGB method. Most of the members in the cluster are lenticular and elliptical galaxies where a large fraction of visible stars is represented by red giants and therefore the TRGB method proves to be practically the only tool for accurate distance measurement. However, for this we need Hubble Space Telescope images taken with $F814W$ -band exposures no shorter than 5000 s in fields located at the periphery of the galaxies rather than at its center.

Acknowledgements Based on observations with the NASA/ESA Hubble Space Telescope, obtained at the Space Telescope Science Institute, which is operated by AURA, Inc. under contract No. NAS5-26555. These observations are associated with proposals 10131, 10543, 12532, 12989 and 13731.

References

- M. Arnaboldi, J. A. L. Aguerri, N. R. Napolitano, et al., 2002, *AJ*, 123, 760. [10](#)
- S. Bird, W. E. Harris, J. P. Blakeslee, and C. Flynn, 2010, *A&A*, 524, A71. [7](#), [10](#)
- N. Caldwell, 2006, *ApJ*, 651, 822. [2](#), [16](#)
- A. Dolphin, 2016, *DOLPHOT: Stellar photometry*. [4](#)
- P. R. Durrell, R. Ciardullo, J. J. Feldmeier, et al., 2002, *ApJ*, 570, 119. [10](#)
- P. R. Durrell, B. F. Williams, R. Ciardullo, et al., 2007, *ApJ*, 656, 746. [15](#)
- H. C. Ferguson, N. R. Tanvir, and T. von Hippel, 1998, *Nature*, 391, 461. [10](#)
- L. Ferrarese, J. R. Mould, R. C. Kennicutt, Jr., et al., 2000, *ApJ*, 529, 745. [10](#)
- P. Fouqué, J. M. Solanes, T. Sanchis, and C. Balkowski, 2001, *A&A*, 375, 770. [13](#), [16](#), [17](#)
- R. A. Ibata, G. F. Lewis, A. W. McConnachie, et al., 2014, *ApJ*, 780, 128. [9](#)
- I. S. Jang and M. G. Lee, 2014, *ApJ*, 795, L6. [15](#)
- S. Janowiecki, J. C. Mihos, P. Harding, et al., 2010, *ApJ*, 715, 972. [2](#)
- Y. Ko, H. S. Hwang, M. G. Lee, et al., 2017, *ApJ*, 835, 212. [10](#)
- J. Kormendy, D. B. Fisher, M. E. Cornell, and R. Bender, 2009, *ApJS*, 182, 216. [10](#)
- M. G. Lee and I. S. Jang, 2016, *ApJ*, 819, 77. [10](#)
- M. G. Lee and I. S. Jang, 2016, *ApJ*, 822, 70. [10](#)
- M. G. Lee, W. L. Freedman, and B. F. Madore, 1993, *ApJ*, 417, 553. [3](#), [11](#), [14](#)
- A. Longobardi, M. Arnaboldi, O. Gerhard, et al., 2013, *A&A*, 558, A42. [16](#)
- A. Longobardi, M. Arnaboldi, O. Gerhard, and R. Hanuschik, 2015, *A&A*, 579, A135. [10](#), [16](#)
- B. F. Madore and W. L. Freedman, 1995, *AJ*, 109, 1645. [11](#)
- S. Mei, J. P. Blakeslee, P. Côté, et al., 2007, *ApJ*, 655, 144. [17](#)
- J. C. Mihos, P. Harding, J. Feldmeier, and H. Morrison, 2005, *ApJ*, 631, L41. [2](#), [3](#), [16](#)

- J. C. Mihos, P. Harding, C. S. Rudick, and J. J. Feldmeier, 2013, *ApJ*, 764, L20. [9](#)
- J. C. Mihos, S. Janowiecki, J. J. Feldmeier, et al., 2009, *ApJ*, 698, 1879. [10](#)
- M. Montes, I. Trujillo, M. A. Prieto, and J. A. Acosta-Pulido, 2014, *MNRAS*, 439, 990. [9](#)
- E. H. Nielsen, Jr. and Z. I. Tsvetanov, 2000, *ApJ*, 536, 255. [17](#)
- L. J. Oldham and M. W. Auger, 2016, *MNRAS*, 457, 421. [10](#)
- M. Rejkuba, W. E. Harris, L. Greggio, et al., 2014, *ApJ*, 791, L2. [9](#)
- C. S. Rudick, J. C. Mihos, P. Harding, et al., 2010, *ApJ*, 720, 569. [9](#)
- C. S. Rudick, J. C. Mihos, and C. McBride, 2006, *ApJ*, 648, 936. [1](#), [16](#)
- M. M. Shara, T. F. Doyle, T. R. Lauer, et al., 2016, *ApJS*, 227, 1. [10](#), [16](#)
- M. M. Shara, T. Doyle, T. R. Lauer, et al., 2017, *ApJ*, 839, 109. [10](#), [16](#)
- E. F. Schlafly and D. P. Finkbeiner, 2011, *ApJ*, 737, 103. [6](#)
- J. M. Solanes, T. Sanchis, E. Salvador-Solé, et al., 2002, *AJ*, 124, 2440. [17](#)
- P. B. Stetson, 1987, *PASP*, 99, 191. [4](#), [5](#)
- P. B. Stetson, 1994, *PASP*, 106, 250. [4](#)
- N. A. Tikhonov, 2017, *Astronomy Letters*, 43, 21. [1](#), [2](#), [11](#), [15](#), [16](#)
- N. A. Tikhonov and O. A. Galazutdinova, 2009, *Astronomy Letters*, 35, 748. [6](#)
- N. A. Tikhonov, O. A. Galazutdinova, and I. O. Drozdovsky, 2005, *A&A*, 431, 127. [9](#)
- N. A. Tikhonov, O. A. Galazutdinova, and E. N. Tikhonov, 2009, *Astronomy Letters*, 35, 599. [5](#)
- B. F. Williams, R. Ciardullo, P. R. Durrell, et al., 2007a, *ApJ*, 656, 756. [2](#), [3](#), [10](#), [14](#), [16](#)
- B. F. Williams, R. Ciardullo, P. R. Durrell, et al., 2007b, *ApJ*, 654, 835. [10](#)